Efficiency Enhanced Seven-band Omnidirectional Rectenna for RF Energy Harvesting

Efficiency Enhanced Seven-band Omnidirectional Rectenna for RF Energy Harvesting

Yuchao Wang, Jingwei Zhang, Yidan Su, Xianwu Jiang, Cheng Zhang, *Member*, *IEEE*, Lei Wang, *Senior Member*, *IEEE*, Qiang Cheng, *Senior Member*, *IEEE*

***Abstract*—In this paper, a seven-band omnidirectional rectenna is proposed for the first time to harvest RF energy. The designed rectenna operates in the following practical and up-to-date frequency bands: GSM1800 (1.8 GHz), LTE (2.1 GHz), WLAN/Wi-Fi (2.4 GHz and 5.8 GHz) and 5G bands (2.6 GHz, 3.5 GHz and 4.9 GHz). To obtain the multiband rectenna, a novel seven-band rectifier is introduced and composed of three optimized single shunt diode rectifiers in parallel. Overall RF-DC conversion efficiencies as high as 44.4% @ 1.84 GHz, 43.9% @ 2.04 GHz, 45.4% @ 2.36 GHz, 43.4% @ 2.54 GHz, 36.1% @ 3.3 GHz, 32.4% @ 4.76 GHz, and 28.3% @ 5.8 GHz are achieved at an input power level of −10 dBm. Moreover, a broadband omnidirectional monopole antenna is further codesigned with elaborate impedance matching to the rectifier. The antenna can harvest RF energy in the bandwidth of 1.67 GHz ~ 5.92 GHz (S_{11} no more than −10 dB) with stable omnidirectional radiation patterns. By integrating the rectifier and the monopole antenna in a low profile, a prototype of the rectenna was manufactured and tested. The experimental results demonstrate that the proposed rectenna has competitive performance in terms of RF-DC conversion efficiency and band coverage, indicating enormous potential for numerous battery-free or low-power-needed applications in the real world.**

***Index Terms*—Omnidirectional broadband antenna, rectenna, RF energy harvesting, seven-band rectifier.**

This work was supported in part by the National Key Research and Development Program of China (2018YFA0701904, 2017YFA0700201, 2017YFA0700202, 2017YFA0700203, and 2020YFA0710100), the National Natural Science Foundation of China (62101394, 61722106, 62001338 and 61731010), the Fundamental Research Funds for the Central Universities (WUT: 2021IVA064, and 2021IVB029), and the Foundation from the Guangxi Key Laboratory of Optoelectronic Information Processing (GD21203). *(Yuchao Wang and Jingwei Zhang contributed equally to this work.) (Corresponding authors: Xianwu Jiang; Cheng Zhang; Cheng Qiang.)*

Yuchao Wang, Jingwei Zhang, Xianwu Jiang, and Cheng Zhang are with the Hubei Engineering Research Center of RF-Microwave Technology and Application, School of Science, Wuhan University of Technology, Wuhan 430070, China (e-mail: yuchao9629@whut.edu.cn; j_zhang@whut.edu.cn; xwjiang@whut.edu.cn; czhang2020@whut.edu.cn).

Yidan Su is with the School of Engineering, the University of Manchester, Manchester, M13 9PL, United Kingdom (e-mail: ethan_su@126.com).

Lei Wang is with the School of Engineering and Physical Sciences, Institute of Sensors, Signals and Systems, Heriot-Watt University, EH14 4AS, United Kingdom (e-mail: Lei.Wang@hw.ac.uk).

Qiang Cheng is with the State Key Laboratory of Millimeter Waves, Southeast University, Nanjing 210096, China (e-mail: qiangcheng@seu.edu.cn).

I. Introduction

With the development of wireless communication technology, there are an increasing number of low-power electronic devices used in applications such as the Internet of Things (IoT), smart cities and wireless sensor networks. Replacing batteries in these low-power electronic devices is a time-consuming and expensive task. In addition, improper disposal of used batteries can result in environmental pollution [1-4]. Hence, there has been widespread interest in harvesting energy from the surrounding environment to power low-power electronic devices. Compared to wind, solar and kinetic energy harvesting, RF energy harvesting for powering electronic devices has the advantage of being implantable and sustainable [5]. Moreover, with the development of 5G communication technology, the number of RF sources in the surrounding environment, such as 5G communication base stations and Wi-Fi, has increased significantly, which means that harvesting RF energy to power devices is more feasible [6].

As the core component in RF energy harvesting, the role of the rectenna is to convert RF power into DC power for output. Typical rectennas consist of a rectifier and a receiver antenna, and the overall efficiency is an important parameter in assessing the performance of a rectenna [7]. Rectennas with high RF-DC conversion efficiency have been reported continuously in recent years [8]-[11]. For example, a rectenna that integrated a filtering function on the receiving antenna was reported in [12] to improve the overall RF-DC conversion efficiency by preventing the harmonics of the diode embedded in the rectifier from being reradiated through the antenna, whereas it was difficult to design a broadband filter antenna. In [13], a classical F-class rectifier was demonstrated to reduce diode losses by modulating the voltage and current waveforms across the diode. However, the complex matching network introduces a large loss, hindering the further improvement in the total RF-DC conversion efficiency. To solve this problem, the matching network between the receiving antenna and the rectifier was removed in [14], that is, directly matching the receiving antenna conjugately with the rectifier to eliminate the loss induced by the matching network. However, it is not feasible to measure the performance of the rectifier independently since the input impedance of the rectifier is not

matched to 50 Ω. Many studies have been devoted to reducing the losses in the rectifier to improve the RF-DC conversion efficiency of the rectifier [12]-[14]. However, the electromagnetic energy at a single frequency is still limited, which hinders its practical applications due to the low DC output power. Hence, multiband rectennas are naturally a promising choice.

Note that the frequency bands of RF energy in the surrounding environment are usually discontinuous, which is a barrier in designing broadband rectifiers that can operate over multiple frequency bands due to the nonlinear impedance characteristics of the diodes [15]-[24]. Therefore, multiband rectennas that can harvest RF energy from multiple frequency bands have attracted considerable interest in the energy field [20], [25]-[28]. For example, a broadband frequency-selectable rectenna was proposed in [20] which operates at four different frequency bands that are selectable from 1.1 to 2.7 GHz and shows great potential in high level RF power harvest. Furthermore, a triband rectifier was designed in [25] by using a three-branch matching circuit, but the RF-DC conversion efficiency of the rectifier was low due to the complexity of the matching network, which introduced more dielectric and conductor losses. Another triband rectenna was demonstrated in [26] to increase RF-DC conversion efficiency at low RF power levels. However, the RF-DC conversion efficiency is lower at 3.5 GHz due to impedance mismatch between the rectifier and the receiving antenna as well as the lower radiation efficiency of the proposed antenna. In addition, a quadband rectifier was proposed in [27] to achieve energy harvesting at 1.3 GHz, 1.7 GHz, 2.4 GHz and 3.6 GHz. However, its RF-DC conversion efficiency was unsatisfactory, as the input power was at low levels. In the meantime, a novel six-band rectenna (0.55 GHz, 0.75 GHz, 0.9 GHz, 1.85 GHz, 2.15 GHz, and 2.45 GHz) was proposed in [28] to harvest RF energy from more frequency bands. Although with the help of an improved impedance matching technique, the rectenna can provide a high RF-DC conversion efficiency at low input power levels, only five bands (0.55 GHz, 0.75 GHz, 0.9 GHz, 1.85 GHz, and 2.3 GHz) can be observed in experimental results due to the unknown parasitic behavior of the surface mount technology (SMD) components used in the circuit and inaccurate package parameters of the diode. Furthermore, a novel eight-band rectenna (0.84 GHz, 1.29 GHz, 1.68 GHz, 3.08 GHz, 3.45 GHz, 4.31 GHz, 5.11 GHz, and 5.49 GHz) was proposed in [29] by designing an eight-band matching network within a single branch. However, the RF-DC conversion efficiency was only 13.5%, 3.3%, and 12.68% at 4.31 GHz, 5.11 GHz, 5.49 GHz at an input power of −10 dBm due to poor matching performance. To date, great improvements have been made in multiband rectifiers for collecting extra electromagnetic power from free space. However, multiband rectifiers that can consider high frequencies, such as WLAN/Wi-Fi and 5G bands [30]-[35], are still lacking. Of course, how to enhance the RF-DC conversion efficiency of each operation band is a long-standing problem that needs to be solved.

Herein, to address the problems mentioned above, we present a new seven-band omnidirectional rectenna for omnidirectional harvesting of RF energy from the surrounding environment in the GSM1800 (1.8 GHz), LTE (2.1 GHz), WLAN/Wi-Fi (2.4 GHz and 5.8 GHz) and 5G bands (2.6 GHz, 3.5 GHz and 4.9 GHz). First, a seven-band rectifier is designed by connecting three optimized single shunt diode rectifiers in parallel. The measured reflection coefficient (S_{11}) and RF-DC conversion efficiency are in good agreement with the simulated results. In the next step, a broadband omnidirectional receiving antenna is independently given out by slotting in the ground. The measured results show that the proposed antenna can receive RF energy omnidirectionally in a bandwidth of 1.67 GHz ~ 5.92 GHz, meeting the demand of the rectifier. Finally, the designed rectifier is integrated with the antenna to evaluate the performance of the proposed seven-band omnidirectional rectenna. The experimental results show that the rectenna can operate normally at an input power of −20 dBm ~ 5 dBm, and the highest RF-DC conversion efficiencies of the proposed rectenna in each frequency band are 49% @ 1.84 GHz, 51% @ 2.04 GHz, 52% @ 2.36 GHz, 53% @ 2.54 GHz, 46% @ 3.3 GHz, 45% @ 4.76 GHz and 35% @ 5.8 GHz at input power levels of 5 dBm, 4 dBm, 4 dBm, 4 dBm, 4 dBm, 6 dBm, and 4 dBm, respectively. To the best of our knowledge, the proposed rectenna is the first design to cover such a wide range of frequencies with a relatively constant high conversion efficiency, especially including the up-to-date 5G bands.

The rest of this paper is organized as follows. Section II introduces the design process and measured results of the rectifier. An omnidirectional broadband-receiving antenna design is discussed in Section III. The experimental results of the rectenna are presented in Section IV. Finally, conclusions are drawn in Section V.

II. Seven-Band Rectifier

The circuit topology of the seven-band rectifier proposed in this paper is shown in Fig. 1(d). The designed seven-band rectifier is constructed with three different rectifier branches in parallel to cover the predesigned frequency bands while maintaining a small size. To implement the multiband function, first, three rectifiers (Figs. 1(a-c)) are designed to capture spatial EM energy at different frequencies. Note that once connected in parallel, the input impedance of each branch will be different from that of the initially designed single shunt diode rectifier. Therefore, some parameters of the dual-band rectifier (Figs. 1(a) and 1(c)) and the triband rectifier (Fig. 1(b)) are studied for the following assembling. Second, the three designed rectifiers are connected in parallel to compose a seven-band rectifier, as shown in Fig. 1(d), through global optimization. Finally, the designed seven-band rectifier is fabricated and measured to evaluate its overall performance. The entire design process is described as follows.

A. Three Single Shunt Diode Rectifiers

Each rectifier branch consists of a rectifier diode, a transmission line at the front of the diode, a DC-pass filter, a matching network, and a load [36]-[40]. In a rectifier, the energy loss of the diodes is the primary factor that can affect the overall RF-DC conversion efficiency of the total system

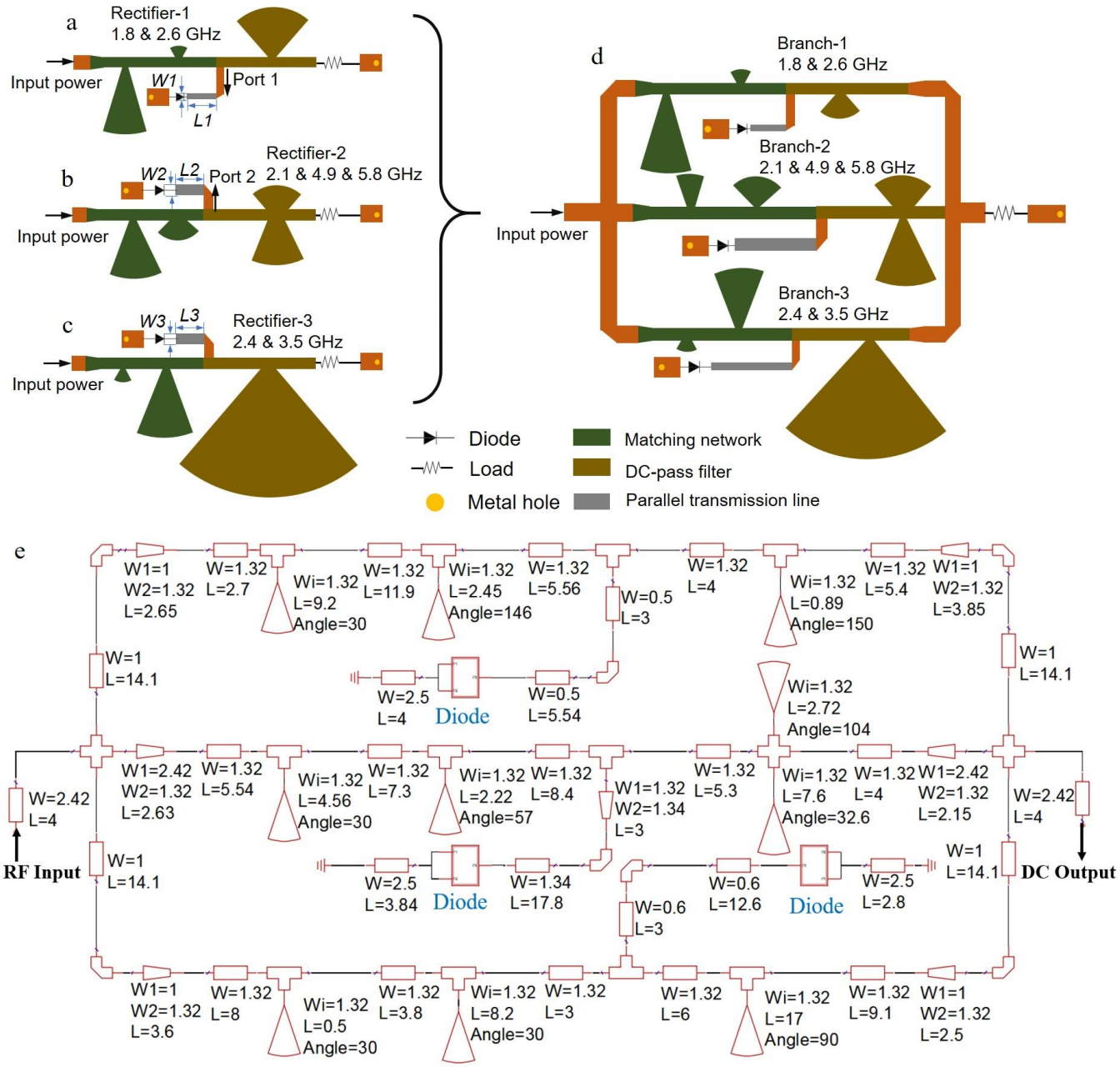

Fig. 1. (a-d) Design process and topology of the proposed rectifier. (e) ADS circuit and detailed dimensions of the proposed rectifier (Unit: mm).

[41]-[45]. Therefore, the three different rectifier branches all use the structure of a single shunt diode rectifier, which induces lower losses than those of voltage double rectifiers and single series diode rectifiers [46]-[50]. In the meantime, the Schottky diode SMS7630 [51] is chosen as the rectifier diode due to its low bias voltage requirements at low power input levels and low losses (forward bias voltage: 60 mV ~ 120 mV at 0.1 mA).

Two transmission lines and a radial stub are adopted to build the dual-band DC-pass filter, of which the input impedance can be adjusted to confine fundamental frequency energy through the load by changing the length of the transmission line and the radial stub (Fig. 1). In the meantime, to realize a compact circuit, the triband DC-pass filter is designed with two transmission lines and two radial stubs, where the sum of the lengths of the two radial stubs is equivalent to the length of the radial stub in a dual-band rectifier. In addition, the microstrip line at the front of the diode can adjust the input impedance of port 1 and port 2 to allow more RF energy to enter the diode to improve the RF-DC conversion efficiency of the rectifier.

Of course, the corresponding matching network is required to match the input impedance of the three designed rectifiers to the widely used 50 Ω impedance. Here, a conventional Π-type matching network is elaborately designed to link the predesigned dual/triband DC-pass filter with the input radio energy. Note that the radial stubs are selected to replace the open microstrip lines to increase the bandwidth of the resonance frequency, leading to the improvement in the matching performance.

In the following, according to the design aims, the three different rectifiers are optimized by utilizing Advanced Design

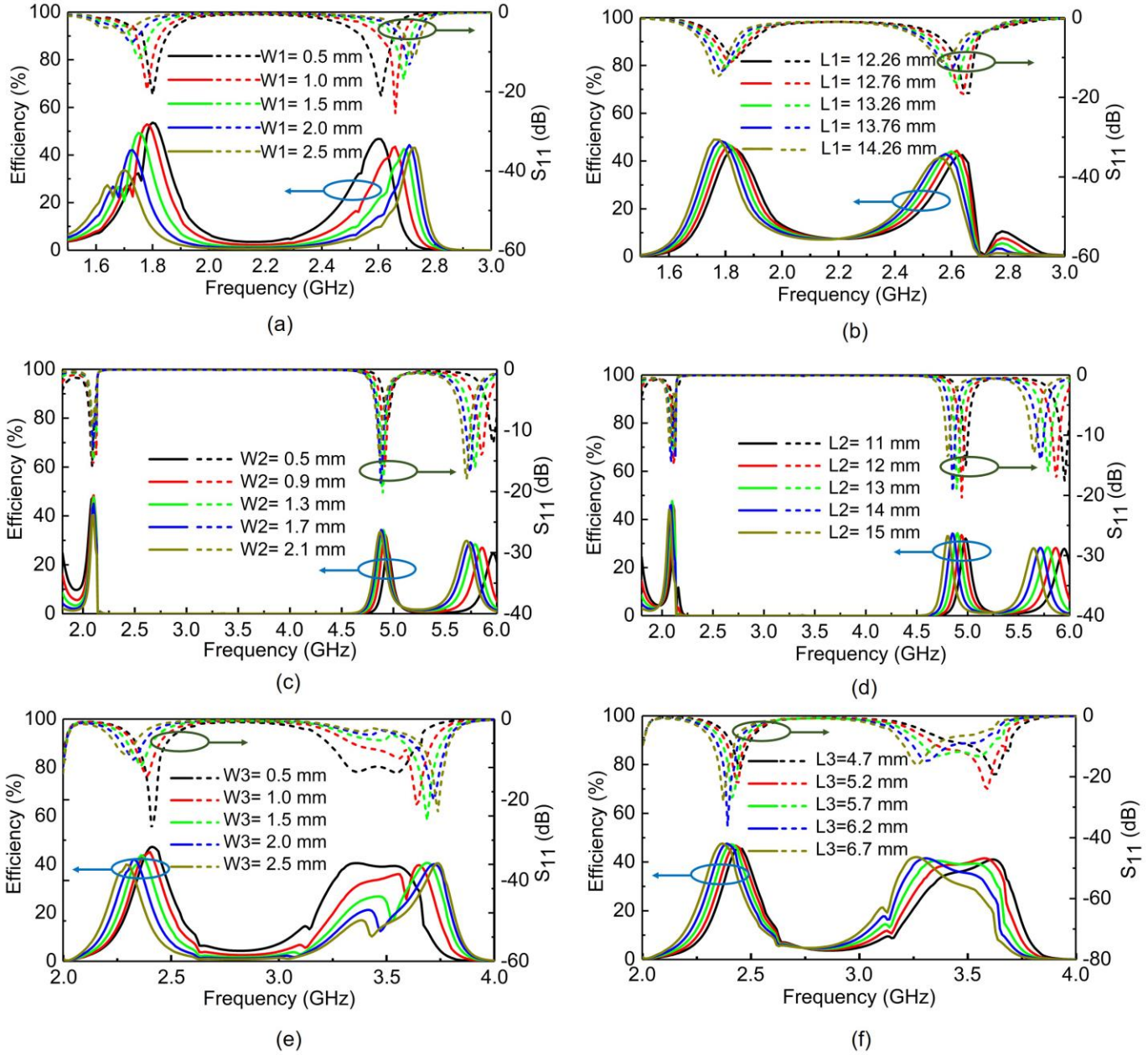

Fig. 2. Simulated RF-DC conversion efficiency and reflection coefficient of the dual-band rectifier (Rectifier-1) with different values of W1 (a) and L1 (b). Simulated RF-DC conversion efficiency and reflection coefficient of the triband rectifier (Rectifier-2) with different values of W2 (c) and L2 (d). Simulated RF-DC conversion efficiency and reflection coefficient of the dual-band rectifier (Rectifier-3) with different values of W3 (e) and L3 (f).

System (ADS) software. For Rectifier-1 and Rectifier-3, the operation frequencies are approximately [1.8 GHz, 2.6 GHz] and [2.4 GHz, 3.5 GHz]. Rectifier-2 can take effect at 2.1 GHz, 4.9 GHz, and 5.8 GHz.

To date, the three rectifiers have been realized at different working frequencies as desired. In the next section, some parameters will be studied to examine their effect on the dual-band rectifier and the triband rectifier. The corresponding results will provide useful guidelines to optimize the performance of the total seven-band rectifier.

B. Dual-band Rectifier

In this section, the effect of structural parameters, including W1 and L1, on the reflection coefficient and RF-DC conversion efficiency of Rectifier-1 (Fig. 1(a)) is shown in Figs. 2(a-b). With increasing W1, the first resonant frequency of Rectifier-1 shifts to a lower frequency, and the second resonant frequency moves in the opposite direction (high frequency). In addition, the performance of Rectifier-1 worsens in terms of the reflection coefficient and the RF-DC conversion efficiency at the first resonant frequency, but little effect on the second resonant frequency can be found during the same process.

Furthermore, the effect of the length of L1 is also studied, and the corresponding simulated results are illustrated in Fig. 2(b). It is obvious that as L1 increases, both resonant frequencies shift toward lower frequencies. Note that the reflection coefficient at the first resonant frequency gradually decays but enhances for the second peak. Similar phenomena

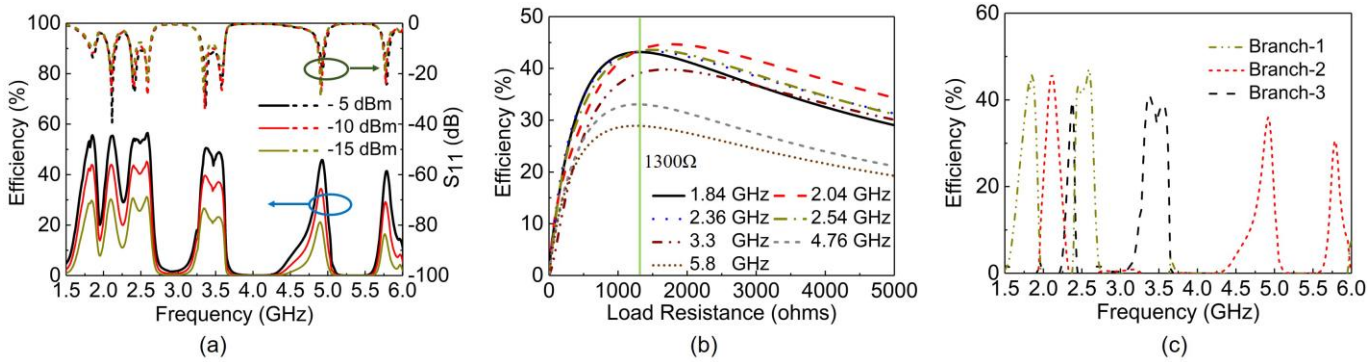

Fig. 3. (a) Simulated RF-DC conversion efficiency and reflection coefficient of the proposed rectifier at three input power levels of −5 dBm, −10 dBm and −15 dBm at a load resistance of 1300 Ω. (b) Simulated RF-DC conversion efficiency of the proposed rectifier versus load resistance at seven bands at an input power of −10 dBm. (c) Simulated RF-DC conversion efficiency of the three branches at the input power level of −10 dBm.

can be observed in Fig. 2(b) with regard to the RF-DC conversion efficiency due to the worse performance of the reflection coefficient. Since the basic structure of Rectifier-3 is similar to that of Rectifier-1, an approximate conclusion can be drawn, as shown in Figs. 2(e-f).

C. Triband Rectifier

In this section, the three-band rectifier (Fig. 1(b)) is studied, and the effect of W2 and L2 on the rectifier is illustrated in Figs. 2(c-d). With increasing W2, the first resonant frequency barely shifts, but the reflection coefficient and RF-DC conversion efficiency worsen. At the same time, there is a small shift at the second resonant frequency and a large shift at the third resonant frequency. Therefore, the third resonant frequency of the triband rectifier can be independently and precisely adjusted by changing the value of W2.

L2 with five different values, 11, 12, 13, 14 and 15 mm, is analyzed, and the corresponding simulated results are shown in Fig. 2(d). The simulation results show that the first resonant frequency also cannot be moved by increasing L2, while the second and third resonant frequencies shift toward lower frequencies. In addition, the performance of Rectifier-3 hardly changes in terms of the reflection coefficient and the RF-DC conversion efficiency at the first resonant frequency and the second resonant frequency. An interesting phenomenon can be observed by studying the third resonant frequency in Fig. 2(d). With increasing L2, the performance of Rectifier-3 becomes better in terms of the reflection coefficient at the third resonant frequency but that in terms of the RF-DC conversion efficiency holds steady.

D. Seven-band Rectifier

Ultimately, the seven-band rectifier is obtained through global optimization in ADS with the help of the abovementioned conclusion drawn in Section B and Section C. The corresponding impedance matching networks are deliberately designed at the same time. The final structure of the optimized rectifier is shown in Fig. 1(d). The ADS circuit and detailed dimensions of the proposed rectifier are shown in Fig. 1(e). The finally simulated reflection coefficient and RF-DC conversion efficiency of the optimized seven-band rectifier at three input power levels of −5 dBm, −10 dBm and −15 dBm are depicted in Fig. 3(a). The proposed rectifier works well in seven predesigned frequency bands (1.8 GHz, 2.1 GHz, 2.4 GHz, 2.6 GHz, 3.5 GHz, 4.9 GHz and 5.8 GHz), covering the GSM1800, LTE, WLAN/Wi-Fi and 5G bands. To study the effect of varying the load resistance on the efficiency, the simulated RF-DC conversion efficiency of the proposed rectifier versus load resistance at seven bands for an input power of −10 dBm is shown in Fig. 3(b). The efficiency first increases and then decreases as the load resistance increases, and the RF-DC conversion efficiencies at predesigned operation bands nearly all reach the maximum values at ~1300 Ω. Therefore, 1300 Ω is chosen as the load resistance of the rectifier. In addition, the conversion efficiency is relatively high overload resistances from 500 to 5000 Ω. Compared to other published articles (Table I on Page 9), the designed seven-band rectifier performs better comprehensively considering RF-DC conversion efficiency and the number of frequency bands.

In addition, the simulated RF-DC conversion efficiency of the three branches at an input power level of −10 dBm is presented to study the contribution of the three branches, as shown in Fig. 3(c). Nearly the whole RF power flows only into the corresponding rectifier branches and can be converted to DC power with a conversion rate of ~40%. Little RF power is converted to DC power by the other two branches, even though the three branches are connected in parallel. That is, the total rectified power across the load is due only to the corresponding branch.

To verify our design, a prototype with a size of 54 mm × 42 mm is printed on a low-cost Duriod 5880 substrate with a relative permittivity of 2.2, loss tangent of 0.0009 and thickness of 0.787 mm, as shown in Fig. 4(a). The reflection coefficient of the rectifier is measured with a vector network analyzer (VNA, Agilent E5072A). The measured results at three different input power levels are shown in Fig. 4(b). Although little discrepancy can be observed with regard to S_{11}, the measured results (Fig. 4(b)) are still consistent with the simulated results (Fig. 3(a)), verifying the excellent performance of our design. The source of the error is analyzed here. We think that the unknown parasitic behavior of the diode and SubMiniature version A (SMA) used in the circuit is the main factor that induces the difference between the measured and simulated results. In addition, the simulation package

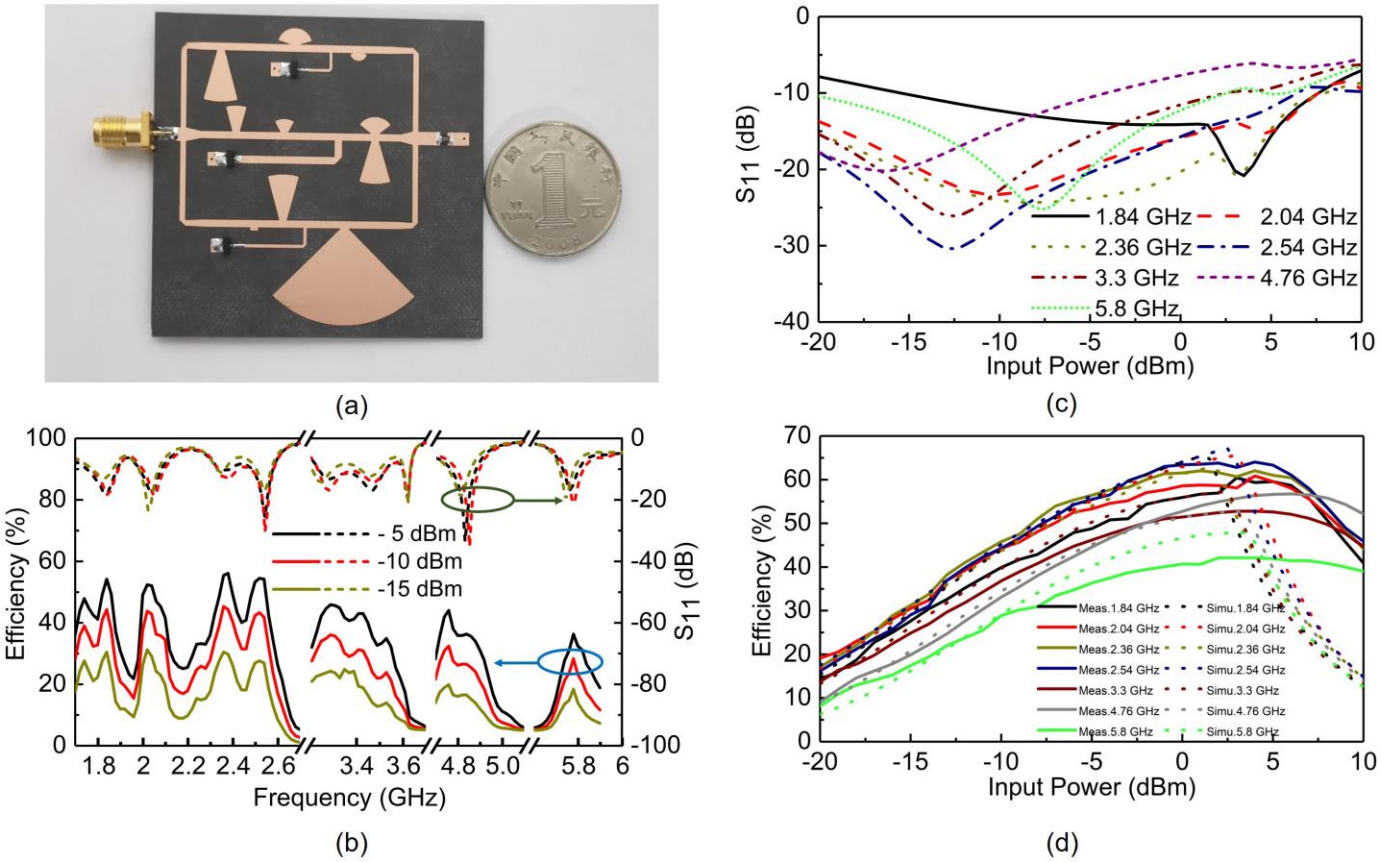

Fig. 4. (a) Fabricated prototype of the proposed seven-band rectifier. (b) Measured RF-DC conversion efficiency and reflection coefficient of the proposed rectifier at three input power levels of −5 dBm, −10 dBm and −15 dBm for a load resistance of 1300 Ω. (c) Simulated S_{11} of the proposed rectifier versus input power level at seven frequencies for a load resistance of 1300 Ω. (d) Measured and simulated RF-DC conversion efficiency of the proposed rectifier versus input power level at seven frequencies for a load resistance of 1300 Ω.

parameters of the diode are also different from the actual parameters.

The RF-DC conversion efficiency can be obtained by using the following equation:

$$Efficiency = \frac{V_{out}^2}{R \times P} \tag{1}$$

where R is the optimal load resistance of the rectifier (1300 Ω), P is the input power provided by the signal generator, and V_{out} is the voltage across the load resistance. The measured RF-DC conversion efficiency as a function of frequency is depicted in Fig. 4(b) at three input power levels for a load resistance of 1300 Ω. Obviously, the rectifier has a high RF-DC conversion efficiency in the seven frequency bands. Comparing the measured result with the simulation, the measured RF-DC conversion efficiency of the rectifier is lower than the simulation result, and the frequency has a smaller deviation. This is due to welding errors and the inaccuracy of the nonlinear model of the diode. In addition, Fig. 4(b) shows that the efficiency at low frequency is greater than the efficiency at high frequency at the same input power. This is due to the increased losses of the diode and dielectric substrate with increasing frequency.

The simulated S_{11} as a function of the input power level is shown in Fig. 4(c) at seven different frequencies. The rectifier is well matched with incident EM waves at 2.1 GHz, 2.4 GHz, 2.6 GHz, 3.5 GHz, 4.9 GHz, and 5.8 GHz when the input power range is −20 dBm to −5 dBm. At 1.8 GHz, the matching performance of the rectifier decreases when the input power is less than −15 dBm due to the nonlinear characteristics of Schottky diode. The RF-DC conversion efficiency as a function of input power at seven different frequencies is depicted in Fig. 4(d), where the RF-DC conversion efficiencies of the rectifier are 44.4% @ 1.84 GHz, 43.9% @ 2.04 GHz, 45.4% @ 2.36 GHz, 43.4% @ 2.54 GHz, 36.1% @ 3.3 GHz, 32.4% @ 4.76 GHz, and 28.3% @ 5.8 GHz at an input power level of −10 dBm. As the input power level increases, the RF-DC conversion efficiency gradually increases at the seven designed frequency bands and decreases sharply as the input power level reaches a threshold value (3 dBm @ 1.84 GHz, 4 dBm @ 2.04 GHz, 4 dBm @ 2.36 GHz, 4 dBm @ 2.54 GHz, 4 dBm @ 3.3 GHz, 5 dBm @ 4.76 GHz and 4 dBm @ 5.8 GHz). This is due to the voltage across the Schottky diode exceeding the reverse breakdown voltage when the input power is too high, resulting in a rapid increase in diode losses. Therefore, the rectifier can work normally at an input power level of −20 dBm to 4 dBm.

III. Omnidirectional Broadband Antenna

A. Antenna Design and Analysis

A seven-band rectifier is designed in Section II. At the same

This article has been accepted for publication in a future issue of this journal, but has not been fully edited. Content may change prior to final publication. Citation information: DOI 10.1109/TAP.2022.3177492, IEEE Transactions on Antennas and Propagation

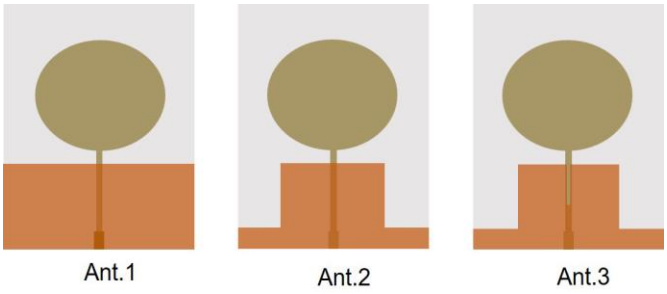

Fig. 5. Evolution of the antenna design

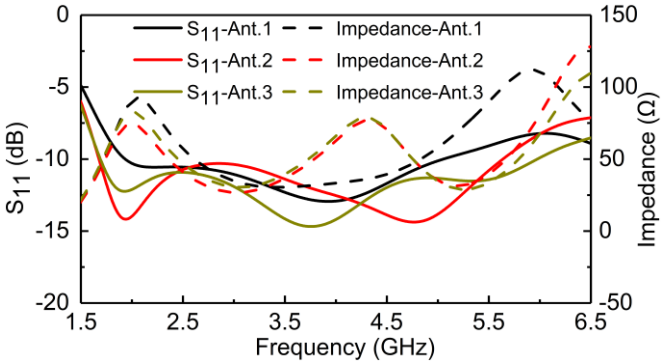

Fig. 6. Simulated reflection coefficient and impedance of the antenna with three ground planes.

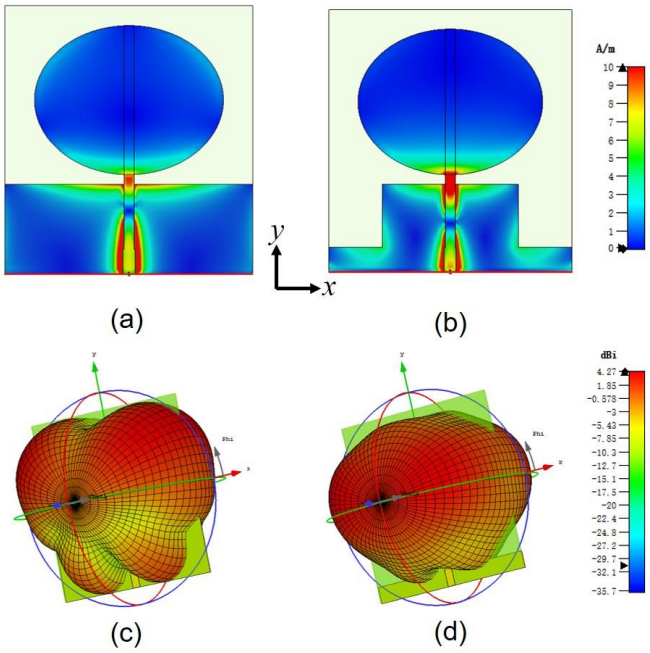

Fig. 7. Surface current distribution of the two antennas at 5.8 GHz: (a) Ant. 1 and (b) Ant. 2. Evolution of the 3-D radiation pattern at 5.8 GHz: (c) Ant. 1 and (d) Ant. 2.

time, a receiving antenna is needed to harvest RF energy at the corresponding seven frequency bands. To simultaneously harvest RF energy at multiple frequency bands from modern communication systems, a broadband antenna is a very popular scenario. Additionally, omnidirectional radiation properties are desirable due to the randomness of RF energy in the surrounding environment. A monopole antenna is selected due

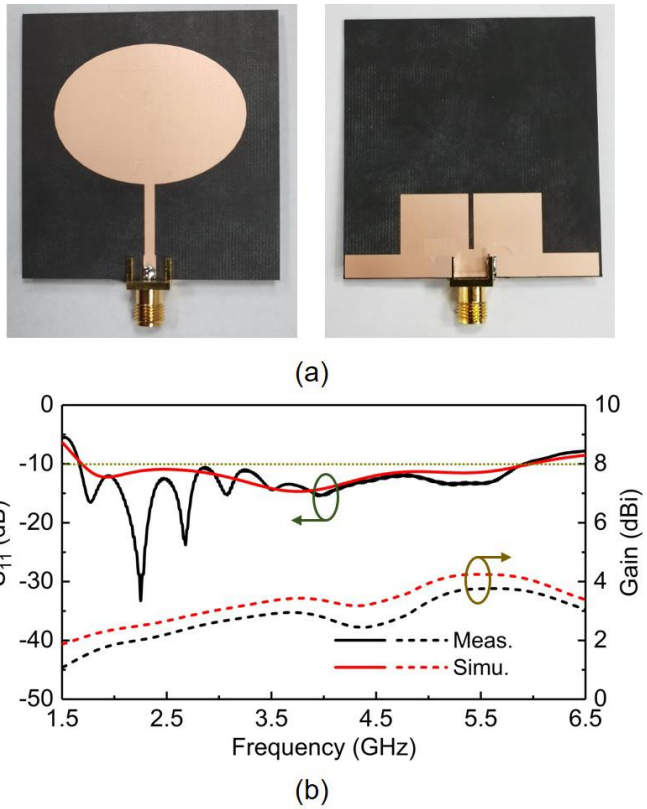

Fig. 8. (a) Fabricated prototype of the proposed omnidirectional antenna. (b) Measured and simulated reflection coefficient and realized gains of the proposed antenna.

to its broad impedance bandwidth and broad beam width. A conventional monopole antenna has omnidirectional radiation characteristics at low frequency. However, the omnidirectional radiation performance will change with frequency due to the change in the surface current distribution.

In this section, a broadband omnidirectional monopole antenna with a size of 54 × 50 mm^2 is proposed based on a slotted ground plane. The surface current distribution of the antenna changes with the introduction of a slotted ground plane, which is advantageous for improving the performance of impedance bandwidth and omnidirectional radiation. The design process is studied by utilizing computer simulation technology (CST) software.

The three different geometries of the antenna during the design evolution are given in Fig. 5. The simulated S_{11} and impedance of the three antennas are studied, as shown in Fig. 6. The impedance bandwidth (S_{11}<−10 dB) of Ant. 1 with the conventional ground plane is 1.9 GHz ~ 5.04 GHz. With slotting at the edge of the ground plane, the impedance of Ant. 2 is adjusted to approximately 50 Ω at 4.7 GHz ~ 5.6 GHz. The impedance bandwidth of Ant. 2 can reach 1.67 GHz ~ 5.63 GHz. Furthermore, the impedance of the antenna (Ant. 3) is reduced at 5.5 GHz ~ 6.5 GHz by slotting at the middle of the ground plane, which improves the impedance bandwidth of the antenna (Ant. 3) at high frequency. Note that the impedance bandwidth of the current antenna (Ant. 3) is 1.69 GHz ~ 5.97 GHz, covering the seven frequency bands of the rectifier.

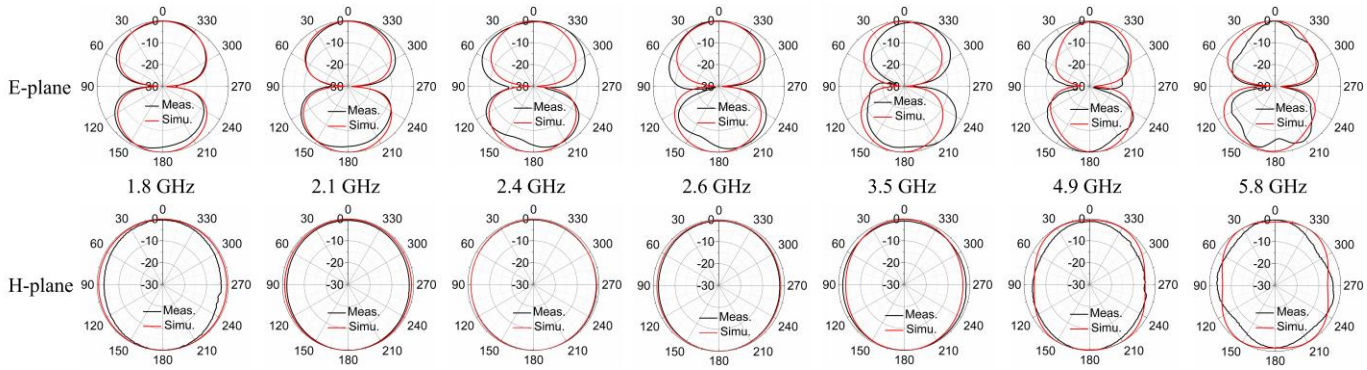

Fig. 9. Measured and simulated 2-D radiation patterns of the antenna.

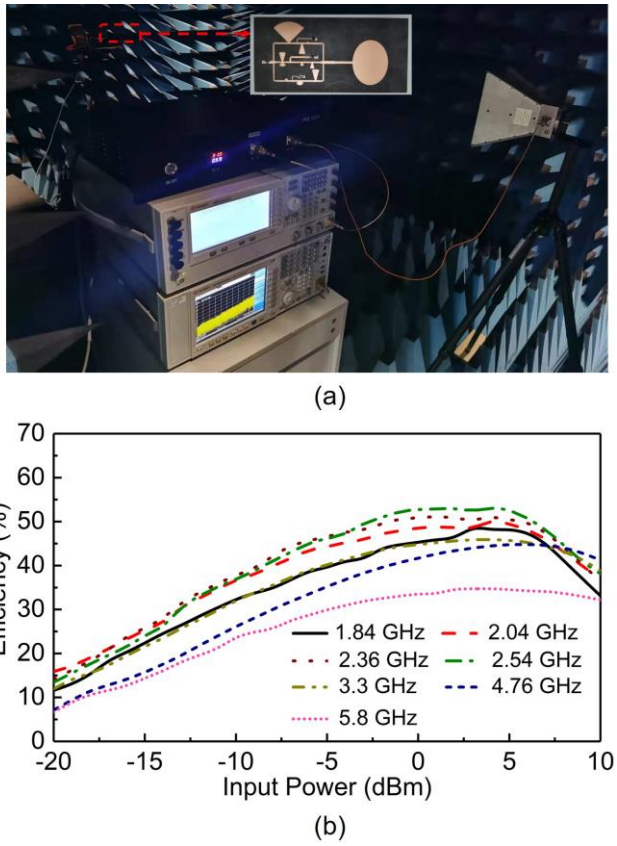

Fig. 10. (a) Measurement setup for the proposed rectenna. The rectenna direction is tuned to match with its maximum gain direction. The fabricated prototype rectenna is shown as well. (b) Measured RF-DC conversion efficiency of the proposed rectenna versus input power level for a load resistance of 1300 Ω.

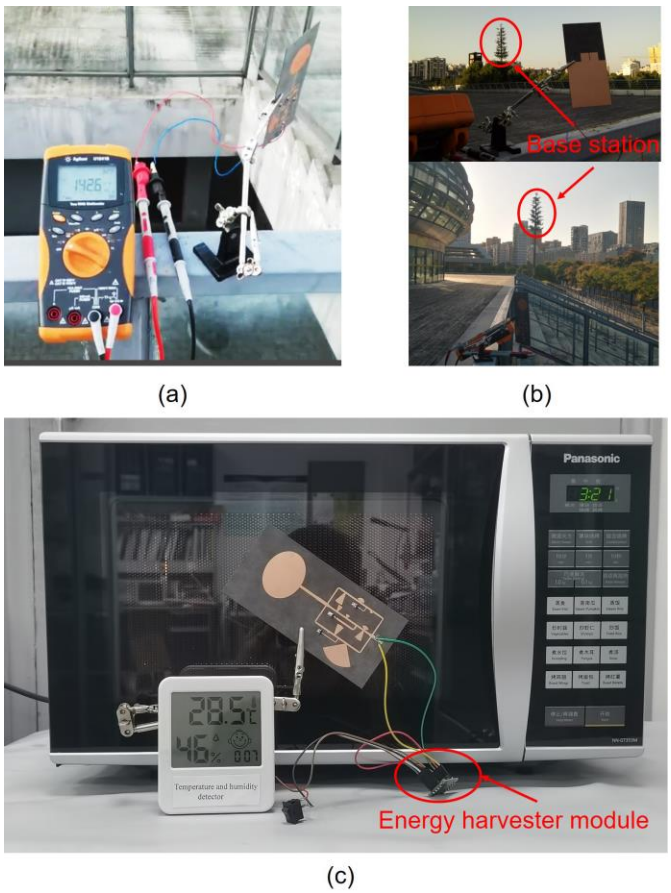

Fig. 11. (a) The output voltage of the rectenna. (b) Rectenna measurement in an outdoor ambient environment. (c) Example of powering the temperature and humidity detector by using the proposed RF energy harvester.

When the ground plane of the antenna is slotted, the radiation pattern of the antenna will change significantly due to the change in the surface current distribution. To further investigate the effect of the slot on the performance of radiation, the surface current distribution and 3-D radiation pattern of Ant. 1 and Ant. 2 at 5.8 GHz are given in Fig. 7. Fig. 7(a) and Fig. 7(c) show that the surface current of Ant. 1 with a full ground plane is mainly distributed at the upper edge of the ground plane and near the feed line. The radiation pattern has two main radiation wave flaps. As shown in Fig. 7(b), the introduction of edge slotting induces the current distribution at the L-shaped corner of the ground plane and thus reconfigures the radiation pattern of the antenna to omnidirectional radiation.

B. Experimental Results of the Antenna

For evaluation, the proposed optimal antenna is printed on a 0.787 mm-thick Duriod 5880 substrate, as shown in Fig. 8(a), and experiments are performed to estimate its performance. The simulated and measured reflection coefficients of the proposed antenna are shown in Fig. 8(b). The simulated and measured impedance bandwidths (S_{11}<−10 dB) of the antenna are 111.7% centered at approximately 3.83 GHz (1.69 GHz ~ 5.97 GHz) and 111.9% centered at approximately 3.8 GHz (1.67 GHz ~ 5.92 GHz). The simulated and measured realized gains of the antenna are also shown in Fig. 8(b). The simulated and measured 2-D radiation patterns of the proposed antenna at

TABLE I
COMPARISON THE PROPOSED RECTENNA AND RELATED DESIGNS

Ref. (year)	Size of rectifier (mm)	Number of bands	Frequency (GHz)	Maximum RF-DC conversion efficiency of the rectifier at a single frequency	Efficiency of the rectifier at −10 dBm	Radiation direction of antenna at all working bands
[25] (2017)	84×35	3	0.925, 1.82, 2.17	42% @ −10 dBm	42%, 32%, 26%	Directional
[26] (2018)	NR*	3	2, 2.5, 3.5	62% @ −3 dBm	55%, 32%, 20%	Directional
[52] (2020)	81×44	3	1.85, 2.15, 2.48	58% @ −5 dBm	43.4%, 46.5%, 38.4%	Directional
[27] (2017)	51×88	4	1.3, 1.7, 2.4, 3.6	54% @ 10 dBm	23%, 17%, 7%, 5%	NR*
[28] (2016)	35×45	5	0.55, 0.75, 0.98, 1.85, 2.3	53% @ −3 dBm	47%, 42%, 51%, 35%, 37%	Directional
[29] (2021)	NR*	8	0.84, 1.29, 1.68, 3.08, 3.45, 4.31, 5.11, 5.49	63.28% @ 0 dBm	52%, 53%, 25%, 25%, 34%, 13.5%, 3.3%, 12.68%	Omnidirectional
This work (2021)	54×42	7	1.84, 2.04, 2.36, 2.54, 3.3, 4.76, 5.8	64% @ 4 dBm	44.4%, 43.9%, 45.4%, 43.4%, 36.1%, 32.4%, 28.3%	Omnidirectional

NR*: Not Reported

the seven desired frequency bands are given in Fig. 9. The antenna can radiate omnidirectionally in multiple frequency bands, which meets the design requirements. From the above measured results, the antenna can harvest RF energy from a wide angle at multiple frequency bands. Therefore, the antenna is a very suitable receiving antenna for the designed seven-band rectifier.

IV. RECTENNA AND APPLICATIONS

To demonstrate the performance of the proposed seven-band omnidirectional rectenna, we fabricated an integrated rectenna based on the best geometric dimensions, as shown in Fig. 10(a). To evaluate the whole system, the commercial Vivaldi standard horn antenna connected to the signal generator are used as the transmitting antenna. To satisfy the far-field condition, two horn antennas are adopted in the measurement process with the size of 60×244 mm (for 1.84~3.3 GHz) and 69×93 mm (for 4.76 GHz and 5.8 GHz), respectively. The proposed rectenna is used as the receiving antenna, as shown in Fig. 10(a). For this purpose, the transmitting power is calculated from the receiving power measured at the corresponding frequency using standard Friis free-space transmission, as shown in the following equation:

$$P_r = P_t + G_r + G_t + 20\log_{10}\left(\frac{\lambda}{4\pi d}\right) \quad (2)$$

where P_t is the transmitting power of the horn antenna in dBm, P_r is the receiving power of the receiving antenna in dBm, and G_r and G_t are the gains of the receiving antenna and horn antenna, respectively. d is the distance between the horn antenna and the receiving antenna, taken as 2.7 m, and λ is the operating wavelength. All losses (coaxial cable and connectors) are considered at the receiving terminal when calculating the transmitting power. Considering the loss of the antenna, the input power (P) of the rectenna is equal to the value of the receiving power (P_r) divided by the radiation efficiency. Next, the output voltage (V_{out}) of the load on the rectenna is measured with a voltmeter, and the transmit power is measured with a spectrum analyzer (Agilent N9320B). Therefore, the overall RF-DC conversion efficiency of the rectenna can be calculated by substituting these two items (P and V_{out}) into Equation (1) given in the previous section.

The measured RF-DC conversion efficiency of the proposed rectenna as a function of input power is depicted in Fig. 10(b). The seven-band rectenna can receive RF energy and can work well at input power levels of −20 dBm ~ 4 dBm. As the input power increases, the conversion efficiency of the rectenna also increases. When the voltage across the diode is greater than the reverse breakdown voltage, the loss of the rectifier increases sharply, so the efficiency of the rectenna decreases. The highest RF-DC conversion efficiencies of the proposed rectenna in the seven frequency bands are 49% @ 1.84 GHz, 51% @ 2.04 GHz, 52% @ 2.36 GHz, 53% @ 2.54 GHz, 46% @ 3.3 GHz, 45% @ 4.76 GHz and 35% @ 5.8 GHz. Compared with the RF-DC conversion efficiency of the rectifier in Fig. 4(b), that of the rectenna decays due to the energy loss induced by the receiving antenna. The designed rectenna can not only harvest the RF energy of GSM1800 and LTE in the environment but also harvest the RF energy of the 5G frequency band and WLAN/Wi-Fi frequency band.

To further evaluate the performance of the proposed rectenna, we measure the proposed rectenna in a real ambient environment outdoors at Wuhan University of Technology, as shown in Fig. 11(b). The measurement location is at the intersection of two base stations. The measured output DC voltage is approximately 100 mV and can reach 142.6 mV, as shown in Fig. 11(a), which corresponds to an output DC power of 15.6 μW (the load is 1300 Ω). In addition, an example of powering a temperature and humidity detector by using the proposed RF energy harvester is shown in Fig. 11(c). An energy harvester module (BQ25570) is connected to the output end of the designed rectenna to boost the output voltage. As shown in Fig. 11(c), the mentioned device can power the temperature and humidity detector around a working

microwave oven.

A comparison between our rectenna design and some recent rectennas and rectifier designs is given in Table I. Our design is seemingly the only one capable of harvesting energy from ambient signals in all seven frequency bands simultaneously. Although the rectenna in [29] can operate in eight frequency bands, the RF-DC conversion efficiency is very low when the frequency is greater than 4 GHz. Our rectifier maintains a high RF-DC conversion efficiency at an input power level of −10 dBm. The proposed rectenna is better than other published designs in overall performance and is therefore a very good candidate for RF energy acquisition in many practical applications.

V. Conclusion

A seven-band omnidirectional rectenna has been presented both theoretically and experimentally. The design process of the seven-band rectifier is described in detail by a systematic study. The experimental results from a prototype show that the proposed seven-band rectenna has achieved overall high and competitive RF-DC conversion efficiency and multiple frequency-band coverage. The designed rectenna can harvest RF energy around the base station and an output voltage of 142.6 mV in one example. In addition, it can power temperature and humidity sensors in ambient environments. In conclusion, the proposed seven-band rectenna is simple in structure, universal in up-to-date operation bands, and high in conversion efficiency, leading to its promising application in harvesting wireless energy and charging sensors, wearable devices and other IoT scenarios such as smart homes and smart agriculture with sustainable development.

References

[1] B. Patrick Motjolopane and R. van Zyl, "A review of rectenna models for electromagnetic energy harvesting," *Journal of Engine., Design and Techn.*, vol. 7, no. 3, pp. 282-292, Jun. 2009.

[2] T. Paing, E. A. Falkenstein, R. Zane, and Z. Popovic, "Custom IC for ultralow power RF energy scavenging," *IEEE Trans. on Power Electron.*, vol. 26, no. 6, pp. 1620-1626, Jun. 2011.

[3] E. Falkenstein, M. Roberg, and Z. Popovic, "Low-Power wireless power delivery," *IEEE Trans. on Microw. Theory and Techn.*, vol. 60, no. 7, pp. 2277-2286, Jul. 2012.

[4] V. Marian, B. Allard, C. Vollaire, and J. Verdier, "Strategy for microwave energy harvesting from ambient field or a feeding source," *IEEE Trans. on Power Electron.*, vol. 27, no. 11, pp. 4481-4491, Von. 2012.

[5] M. Pinuela, P. D. Mitcheson, and S. Lucyszyn, "Ambient RF energy harvesting in urban and semi-urban environments," *IEEE Trans. on Microw. Theory and Techn.*, vol. 61, no. 7, pp. 2715-2726, May 2013.

[6] Q. Awais, Y. Jin, H. T. Chattha, M. Jamil, H. Qiang, and B. A. Khawaja, "A compact rectenna system with high conversion efficiency for wireless energy harvesting," *IEEE Access*, vol. 6, pp. 35857-35866, Jul. 2018.

[7] C. Song, Y. Huang, J. Zhou, J. Zhang, S. Yuan, and P. Carter, "A high-efficiency broadband rectenna for ambient wireless energy harvesting," *IEEE Trans. on Antennas and Propag.*, vol. 63, no. 8, pp. 3486-3495, Aug. 2015.

[8] T. Matsunaga, E. Nishiyama, and I. Toyoda, "5.8-GHz stacked differential rectenna suitable for large-scale rectenna arrays with DC connection," *IEEE Trans. on Antennas and Propag.*, vol. 63, no. 12, pp. 5944-5949, Dec. 2015.

[9] M.-J. Nie, X.-X. Yang, G.-N. Tan, and B. Han, "A compact 2.45-GHz broadband rectenna using grounded coplanar waveguide," *IEEE Antennas and Wireless Propag. Lett.*, vol. 14, pp. 986-989, Dec. 2015.

[10] S. Ladan, A. B. Guntupalli, and K. Wu, "A high-efficiency 24 GHz rectenna development towards millimeter-wave energy harvesting and wireless power transmission," *IEEE Trans. on Circuits and Systems*, vol. 61, no. 12, pp. 3358-3366, Dec. 2014.

[11] C. H. K. Chin, X. Quan, and C. Chi Hou, "Design of a 5.8-GHz rectenna incorporating a new patch antenna," *IEEE Antennas and Wireless Propag. Lett.*, vol. 4, pp. 175-178, Nov. 2005.

[12] Y. Dong, S. Gao, Q. Luo, S. w. Dong, and G. Wei, "Filtering antennas for energy harvesting in wearable systems," *Intern. Journal of Numerical Modelling: Electron. Networks, Devices and Fields*, vol. 32, no. 6, Jun. 2019.

[13] P. Butterworth, S. Gao, S. F. Ooi, and A. Sambell, "High-efficiency class-F power amplifier with broadband performance," *Micro. and Optical Techn. Lett.*, vol. 44, no. 3, pp. 243-247, Jun. 2005.

[14] C. Song *et al.*, "Matching network elimination in broadband rectennas for high-efficiency wireless power transfer and energy harvesting," *IEEE Trans. on Indust. Electron.*, vol. 64, no. 5, pp. 3950-3961, May 2017.

[15] P. Lu, X.-S. Yang, J.-L. Li, and B.-Z. Wang, "Polarization reconfigurable broadband rectenna with tunable matching network for microwave power transmission," *IEEE Trans. on Antennas and Propag.*, vol. 64, no. 3, pp. 1136-1141, Mar. 2016.

[16] L. Zhang, Y.-C. Jiao, Y. Ding, B. Chen, and Z.-B. Weng, "CPW-Fed broadband circularly polarized planar monopole antenna with improved ground-plane structure," *IEEE Trans. on Antennas and Propag.*, vol. 61, no. 9, pp. 4824-4828, Sep. 2013.

[17] Z. He and C. Liu, "A compact high-efficiency broadband rectifier with a wide dynamic range of input power for energy harvesting," *IEEE Microw. and Wireless Comp. Lett.*, vol. 30, no. 4, pp. 433-436, Apr. 2020.

[18] W. Liu, K. Huang, T. Wang, Z. Zhang, and J. Hou, "A broadband high-efficiency RF rectifier for ambient RF energy harvesting," *IEEE Microw. and Wireless Comp. Lett.*, vol. 30, no. 12, pp. 1185-1188, Dec. 2020.

[19] S. D. Joseph, Y. Huang, and S. S. H. Hsu, "Transmission lines-based impedance matching technique for broadband rectifier," *IEEE Access*, vol. 9, pp. 4665-4672, Dec. 2021.

[20] C. Song, Y. Huang, P. Carter, J. Zhou, S. D. Joseph, and G. Li, "Novel compact and broadband frequency-selectable rectennas for a wide input-power and load impedance range," *IEEE Trans. on Antennas and Propag.*, vol. 66, no. 7, pp. 3306-3316, Jul. 2018.

[21] C. Song, Y. Huang, J. Zhou, and P. Carter, "Improved ultrawideband rectennas using hybrid resistance compression technique," *IEEE Trans. on Antennas and Propag.*, vol. 65, no. 4, pp. 2057-2062, Apr. 2017.

[22] S. Shen, C.-Y. Chiu, and R. D. Murch, "Multiport pixel rectenna for ambient RF energy harvesting," *IEEE Trans. on Antennas and Propag.*, vol. 66, no. 2, pp. 644-656, Feb. 2018.

[23] A. Quddious, S. Zahid, F. A. Tahir, M. A. Antoniades, P. Vryonides, and S. Nikolaou, "Dual-band compact rectenna for UHF and ISM wireless power transfer systems," *IEEE Trans. on Antennas and Propag.*, vol. 69, no. 4, pp. 2392-2397, Apr. 2021.

[24] C. Song, P. Lu, and S. Shen, "Highly efficient omnidirectional integrated multiband wireless energy harvesters for compact sensor nodes of internet-of-things," *IEEE Trans. on Indust. Electron.*, vol. 68, no. 9, pp. 8128-8140, Feb. 2021.

[25] S. Shen, C.-Y. Chiu, and R. D. Murch, "A dual-port triple-band L-probe microstrip patch rectenna for ambient RF energy harvesting," *IEEE Antennas and Wireless Propag. Lett.*, vol. 16, pp. 3071-3074, Jul. 2017.

[26] S. Chandravanshi, S. S. Sarma, and M. J. Akhtar, "Design of triple band differential rectenna for RF energy harvesting," *IEEE Trans. on Antennas and Propag.*, vol. 66, no. 6, pp. 2716-2726, Jun. 2018.

[27] C.-Y. Hsu, S.-C. Lin, and Z.-M. Tsai, "Quadband rectifier using resonant matching networks for enhanced harvesting capability," *IEEE Microw. and Wireless Comp. Lett.*, vol. 27, no. 7, pp. 669-671, Jul. 2017.

[28] C. Song, Yi Huang, Paul Carter, and J Zhou, "A novel six-band dual cp rectenna using improved impedance matching technique for ambient RF energy harvesting," *IEEE Trans. on Antennas and Propag.*, vol. 64, no. 7, pp. 3160-3171, Jul. 2016.

[29] N. Mirzababaee, F. Geran, S. Mohanna, "A radio frequency energy harvesting rectenna for GSM, LTE, WLAN, and WiMAX," *RF and Microwave*,vol. 55, no. 2, pp. 35-42, Mar. 2021.

[30] L. Sun, Y. Li, and Z. Zhang, "Wideband decoupling of integrated slot antenna pairs for 5G smartphones," *IEEE Trans. on Antennas and Propag.*, vol. 69, no. 4, pp. 2386-2391, Apr. 2021.

[31] H. Kim and S. Nam, "Performance enhancement of 5G millimeter wave antenna module integrated tablet device," *IEEE Trans. on Antennas and Propag.*, vol. 69, no. 7, pp. 3800-3810, Jan. 2021.

[32] Y. Cheng and Y. Dong, "Wideband circularly polarized planar antenna array for 5G millimeter-wave applications," *IEEE Trans. on Antennas and Propag.*, vol. 69, no. 5, pp. 2615-2627, Feb. 2021.
[33] X. Ruan and C. H. Chan, "An endfire circularly polarized complementary antenna array for 5G applications," *IEEE Trans. on Antennas and Propag.*, vol. 68, no. 1, pp. 266-274, Jul. 2020.
[34] T. Li and Z. N. Chen, "Shared-surface dual-band antenna for 5G applications," *IEEE Trans. on Antennas and Propag.*, vol. 68, no. 2, pp. 1128-1133, Feb. 2020.
[35] C. Ding, H.-H. Sun, H. Zhu, and Y. Jay Guo, "Achieving wider bandwidth With full-wavelength dipoles for 5G base stations," *IEEE Trans. on Antennas and Propag.*, vol. 68, no. 2, pp. 1119-1127, May 2020.
[36] H. Sun, "An enhanced rectenna using differentially-fed rectifier for wireless power transmission," *IEEE Antennas and Wireless Propag. Lett.*, pp. 1-1, Apr. 2015.
[37] H. Sun and W. Geyi, "A new rectenna with all-polarization-receiving capability for wireless power transmission," *IEEE Antennas and Wireless Propag. Lett.*, vol. 15, pp. 814-817, Aug. 2016.
[38] H. Sun, H. He, and J. Huang, "Polarization-insensitive rectenna arrays with different power combining strategies," *IEEE Antennas and Wireless Propag. Lett.*, vol. 19, no. 3, pp. 492-496, Mar. 2020.
[39] F. Xie, G.-M. Yang, and W. Geyi, "Optimal design of an antenna array for energy harvesting," *IEEE Antennas and Wireless Propag. Lett.*, vol. 12, pp. 155-158, Jan. 2013.
[40] M. Zeng, A. S. Andrenko, X. Liu, Z. Li, and H.-Z. Tan, "A compact fractal loop rectenna for RF energy harvesting," *IEEE Antennas and Wireless Propag. Lett.*, vol. 16, pp. 2424-2427, Jun. 2017.
[41] Z. Ma and G. A. E. Vandenbosch, "Wideband harmonic rejection filtenna for wireless power transfer," *IEEE Trans. on Antennas and Propag.*, vol. 62, no. 1, pp. 371-377, Aug. 2014.
[42] H. Kanaya, S. Tsukamaoto, T. Hirabaru, D. Kanemoto, R. K. Pokharel, and K. Yoshida, "Energy harvesting circuit on a one-sided directional flexible antenna," *IEEE Microw. and Wireless Comp. Lett.*, vol. 23, no. 3, pp. 164-166, Mar. 2013.
[43] M. Wagih, A. S. Weddell, and S. Beeby, "Meshed high-impedance matching network-free rectenna optimized for additive manufacturing," *IEEE Open Journal of Antennas and Propag.*, vol. 1, pp. 615-626, Nov. 2020.
[44] K. Niotaki, S. Kim, S. Jeong, A. Collado, A. Georgiadis, and M. M. Tentzeris, "A compact dual-band rectenna using slot-loaded dual band folded dipole antenna," *IEEE Antennas and Wireless Propag. Lett.*, vol. 12, pp. 1634-1637, Oct. 2013.
[45] H. Sun and W. Geyi, "A new rectenna using beamwidth-enhanced antenna array for RF power harvesting applications," *IEEE Antennas and Wireless Propag. Lett.*, vol. 16, pp. 1451-1454, Dec. 2017.
[46] K. Bhatt, S. Kumar, P. Kumar, and C. C. Tripathi, "Highly efficient 2.4 and 5.8 GHz dual-band rectenna for energy harvesting applications," *IEEE Antennas and Wireless Propag. Lett.*, vol. 18, no. 12, pp. 2637-2641, Dec. 2019.
[47] H. Tafekirt, J. Pelegri-Sebastia, A. Bouajaj, and B. M. Reda, "A sensitive triple-band rectifier for energy harvesting applications," *IEEE Access*, vol. 8, pp. 73659-73664, May. 2020.
[48] X. Li, L. Yang, and L. Huang, "Novel design of 2.45-GHz rectenna element and array for wireless power transmission," *IEEE Access*, vol. 7, pp. 28356-28362, Mar. 2019.
[49] S. Chandravanshi, K. K. Katare, and M. J. Akhtar, "A flexible dual-band rectenna with full azimuth coverage," *IEEE Access*, vol. 9, pp. 27476-27484, Feb. 2021.
[50] S. M. Saeed, C. A. Balanis, C. R. Birtcher, A. C. Durgun, and H. N. Shaman, "Wearable flexible reconfigurable antenna integrated with artificial magnetic conductor," *IEEE Antennas and Wireless Propagation Lett.*, vol. 16, pp. 2396-2399, Jun. 2017.
[51] *Surface Mount Mixer and Detector Schottky Diodes, Data Sheet*, Skyworks Solutions, Inc., Woburn, MA, USA, 2013.
[52] S. Shen, Y. Zhang, C.-Y. Chiu, and R. Murch, "A triple-band high-Gain multibeam ambient RF energy harvesting system utilizing hybrid combining," *IEEE Trans. on Indust. Electron.*, vol. 67, no. 11, pp. 9215-9226, Nov. 2020.

Yuchao Wang received the B.S. degree from the Wuhan University of Technology, Hubei, China, in 2018, where he received the M.S. degree in 2021. His research interests include planar antennas, RF energy harvesting, and wireless power transmission.

Jingwei Zhang received the B.S. degree in electrical engineering from the Wuhan University of Technology, Hubei, China, in 2009 and the Ph.D. degree in electrical engineering and electronics from the University of Liverpool, Liverpool, U.K., in 2014. In September 2014, she joined as a Lecturer with the School of Science, Wuhan University of Technology, where she is now an associate professor in RF and Microwave engineering. Her research interests include wireless power transfer and energy harvesting, graphene-based wireless communication, terahertz band communication, and dielectric resonator antennas.

Yidan Su was born in China. She received the BEng degree in Electrical and Electronic Engineering from the University of Manchester, United Kingdom in 2022.

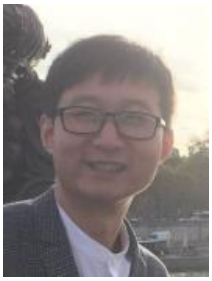

Xianwu Jiang was born in Hunan, China. He received his PhD from Paris-Saclay University in Physics. He joint the faculty of the Wuhan University of Technology where he is currently an Assistant Professor in School of Science.

Cheng Zhang was born in Henan, China. He received the M.S. degree in material science and technology from Wuhan University of Technology, Wuhan, China, in 2015, and the Ph.D degree at the State Key Laboratory of Millimeter Waves, Department of Radio Engineering, Southeast University, Nanjing, in 2019. From August 2020 to present, he is an Assistant Professor in Hubei Engineering Research Center of RF-Microwave Technology and Application, School of Science, Wuhan University of Technology, Wuhan, China. His current research interests are EM energy harvesting, stealth metamaterial/metasurface and multi-physical manipulation. He has authored or co-authored more than fifty publications

(including four highly cited papers), with citation over 900 times.

He was a recipient of the 2020 CHINA TOP CITED PAPER AWARD from IOP Publishing and Top Articles in Device Physics for Applied Physics Letters (two papers). He received the Honor Mention Award for Best Student Paper Contest in 2018 IEEE International Workshop on Antenna Technology (iWAT) and the Appreciation Award of Invited Talk in 2018 IEEE International Conference on Computational Electromagnetics (ICCEM).

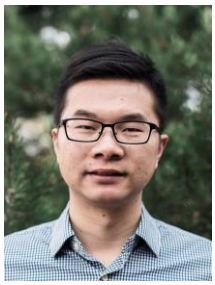

Lei Wang (S'09-M'16-SM'19) received the Ph.D. degree in electromagnetic field and microwave technology from the Southeast University, Nanjing, China in 2015. From September 2014 to September 2016, he was a Research Fellow and Postdoc in the Laboratory of Electromagnetics and Antennas, Swiss Federal Institute of Technology (EPFL) in Lausanne, Switzerland. From October 2016 to November 2017, he was a Postdoc Research Fellow in Electromagnetic Engineering Laboratory of KTH Royal Institute of Technology in Stockholm, Sweden. From November 2017 to February 2020, he was an Alexander von Humboldt scholar in the Institute of Electromagnetic Theory of Hamburg University of Technology (TUHH) in Hamburg, Germany. From March 2020 to present, he is an Assistant Professor in the Institute of Signals, Sensors and Systems of Heriot-Watt University in Edinburgh, United Kingdom. His research includes the antenna theory and applications, active electronically scanning arrays, integrated antennas and arrays, substrate-integrated waveguide antennas, leaky-wave antennas, and wireless propagations.

He was awarded the Chinese National Scholarship for PhD Candidates in 2014 and was granted the Swiss Government Excellence Scholarship to conduct research at EPFL in 2014 too. He was also granted by the Alexander von Humboldt Research Foundation to take research at TUHH in 2016. Moreover, he received the Best Poster Award in 2018 IEEE International Workshop on Antenna Technology (iWAT) and the Best Paper Award in the 5th International Conference on the UK-China Emerging Technologies (UCET2020).

Qiang Cheng (M'15) received the B.S. and M.S. degrees from the Nanjing University of Aeronautics and Astronautics, Nanjing, Jiangsu, China, in 2001 and 2004, respectively, and the Ph.D. degree from Southeast University, Nanjing, in 2008.

In 2008, he joined the State Key Laboratory of Millimeter Waves, Southeast University, where he was involved in the development of metamaterials and metadevices. He is currently a Full Professor with the Radio Department, Southeast University. He leads a group of Ph.D. students and master students in the area of metamaterials, tunable microwaves circuits, microwave imaging, and terahertz systems. He has authored or co-authored more than one hundred publications, with citation over 2000 times

Dr. Cheng was a recipient of the 2010 Best Paper Award from the New Journal of Physics, the Chinas Top Ten Scientific Advances of 2010, and the Second Class National Natural Science Award in 2014. He served as the Vice Chair for the 2008 and 2010 International Workshop on Metamaterials, Nanjing, China.